EVALUATING DRONE TECHNOLOGY TO IDENTIFY ICE CHANGES THAT CAN CAUSE ICE-ROAD HAZARDS

FINAL PROJECT REPORT

by

Eyal Saiet
The Alaska Center for UAS Integration (ACUASI)
The University of Alaska Fairbanks

for

Center for Safety Equity in Transportation (CSET)
USDOT Tier 1 University Transportation Center
University of Alaska Fairbanks
ELIF Suite 240, 1764 Tanana Drive
Fairbanks, AK 99775-5910

In cooperation with U.S. Department of Transportation,
Research and Innovative Technology Administration (RITA)

DISCLAIMER

The contents of this report reflect the views of the authors, who are responsible for the facts and the accuracy of the information presented herein. This document is disseminated under the sponsorship of the U.S. Department of Transportation's University Transportation Centers Program, in the interest of information exchange. The Center for Safety Equity in Transportation, the U.S. Government, and the matching sponsor assume no liability for the contents or use thereof.

TECHNICAL REPORT DOCUMENTATION PAGE

1. Report No.	2. Government Accession No.	3. Recipient's Catalog No.

4. Title and Subtitle	5. Report Date: 2/24/25
EVALUATING DRONE TECHNOLOGY TO IDENTIFY ICE CHANGES THAT CAN CAUSE ICE-ROAD HAZARDS	6. Performing Organization Code

7. Author(s) and Affiliations:	8. Performing Organization Report No.
Eyal Saiet	INE/CSET 25.02

9. Performing Organization Name and Address	10. Work Unit No. (TRAIS)
Center for Safety Equity in Transportation ELIF Building Room 240, 1760 Tanana Drive Fairbanks, AK 99775-5910	11. Contract or Grant No.

12. Sponsoring Organization Name and Address	13. Type of Report and Period Covered
United States Department of Transportation Research and Innovative Technology Administration 1200 New Jersey Avenue, SE Washington, DC 20590	14. Sponsoring Agency Code

15. Supplementary Notes

Report uploaded to:

16. Abstract

Ice roads in Alaska, a form that connects people during the winter months, enable the importing of critical goods and accessibility to medical services. These ice roads span 100 miles or more and are subject to spatial and temporal safety variability during the shoulder seasons and unseasonal warm events of above-freezing temperatures. In this work, we explore using an unmanned aircraft system (UAS) coupled with a ground penetrating radar (GPR) to inspect ice thickness safety and the presence of subsnow liquid overflow, common during winter. We compared our UAS-based GPR with ground-based GPR and nearby ice coring. We found the UAS-based GPR biased compared to the ice cores and the ground-based GPR. Nonetheless, when accounting for this bias, the UAS-based GPR had an RMSE of 5 cm for an ice thickness of 20 to 60 cm. More work is needed to understand the root cause of the UAS-based GPR for measuring ice thickness. The UAS-based GPR also effectively mapped subsnow liquid overflow by measuring the radar return amplitude, which is particularly strong when reflecting between the snow and water layers. Coupling UAS and GPR technology has great promise in conducting ice river safety assessments from a safe location. Still, more work must be done to understand the data's bias.

17. Key Words	18. Distribution Statement
UAS, drones, GPR, river ice, ice roads.	

19. Security Classification (of this report)	20. Security Classification (of this page)	21. No. of Pages	22. Price
Unclassified.	Unclassified.	21	N/A

Form DOT F 1700.7 (8-72) **Reproduction of completed page authorized.**

SI* (MODERN METRIC) CONVERSION FACTORS

APPROXIMATE CONVERSIONS TO SI UNITS				
Symbol	**When You Know**	**Multiply By**	**To Find**	**Symbol**
		LENGTH		
in	inches	25.4	millimeters	mm
ft	feet	0.305	meters	m
yd	yards	0.914	meters	m
mi	miles	1.61	kilometers	km
		AREA		
in^2	square inches	645.2	square millimeters	mm^2
ft^2	square feet	0.093	square meters	m^2
yd^2	square yard	0.836	square meters	m^2
ac	acres	0.405	hectares	ha
mi^2	square miles	2.59	square kilometers	km^2
		VOLUME		
fl oz	fluid ounces	29.57	milliliters	mL
gal	gallons	3.785	liters	L
ft^3	cubic feet	0.028	cubic meters	m^3
yd^3	cubic yards	0.765	cubic meters	m^3
	NOTE: volumes greater than 1000 L shall be shown in m^3			
		MASS		
oz	ounces	28.35	grams	g
lb	pounds	0.454	kilograms	kg
T	short tons (2000 lb)	0.907	megagrams (or "metric ton")	Mg (or "t")
		TEMPERATURE (exact degrees)		
°F	Fahrenheit	5 (F-32)/9 or (F-32)/1.8	Celsius	°C
		ILLUMINATION		
fc	foot-candles	10.76	lux	lx
fl	foot-Lamberts	3.426	$candela/m^2$	cd/m^2
		FORCE and PRESSURE or STRESS		
lbf	poundforce	4.45	newtons	N
lbf/in^2	poundforce per square inch	6.89	kilopascals	kPa

APPROXIMATE CONVERSIONS FROM SI UNITS				
Symbol	**When You Know**	**Multiply By**	**To Find**	**Symbol**
		LENGTH		
mm	millimeters	0.039	inches	in
m	meters	3.28	feet	ft
m	meters	1.09	yards	yd
km	kilometers	0.621	miles	mi
		AREA		
mm^2	square millimeters	0.0016	square inches	in^2
m^2	square meters	10.764	square feet	ft^2
m^2	square meters	1.195	square yards	yd^2
ha	hectares	2.47	acres	ac
km^2	square kilometers	0.386	square miles	mi^2
		VOLUME		
mL	milliliters	0.034	fluid ounces	fl oz
L	liters	0.264	gallons	gal
m^3	cubic meters	35.314	cubic feet	ft^3
m^3	cubic meters	1.307	cubic yards	yd^3
		MASS		
g	grams	0.035	ounces	oz
kg	kilograms	2.202	pounds	lb
Mg (or "t")	megagrams (or "metric ton")	1.103	short tons (2000 lb)	T
		TEMPERATURE (exact degrees)		
°C	Celsius	1.8C+32	Fahrenheit	°F
		ILLUMINATION		
lx	lux	0.0929	foot-candles	fc
cd/m^2	$candela/m^2$	0.2919	foot-Lamberts	fl
		FORCE and PRESSURE or STRESS		
N	newtons	0.225	poundforce	lbf
kPa	kilopascals	0.145	poundforce per square inch	lbf/in^2

*SI is the symbol for the International System of Units. Appropriate rounding should be made to comply with Section 4 of ASTM E380.
(Revised March 2003)

TABLE OF CONTENTS

LIST OF FIGURES

LIST OF TABLES

EXECUTIVE SUMMARY

In Alaska, many villages are disconnected from the state highway and even from major town hubs that offer critical services, such as hospitals, for most of the year. In winter, some of these villages are bridged by ice roads - frozen river sections spanning 100 miles long. These ice roads are cared for and inspected to ensure their safety. However, unseasonal warming events above freezing temperatures and variability of the shoulder season make it overwhelming to ensure the safety of these ice roads.

Manual ice coring is the only way to measure ice thickness and evaluate its quality physically, ideally clear ice without air bubbles. Conversely, ice coring is intensive, laborious work. Noninvasive imaging technology, such as ground-penetrating radar (GPR), is showing promise in evaluating ice thickness. Typically, GPR is towed behind a pedestrian or snowmachine. Both ice coring and monitoring using GPR require being physically on the ice and putting people and equipment at risk.

Here, we introduce an unmanned aircraft system (UAS) coupled with a GPR system to extend the cover of traditional GPR. We found that coupling these technologies enables assessing ice thickness from safety and minimizes exposure risk.

Our UAS GPR was effective in measuring ice thickness where liquid subsnow overflow was absent and effective at mapping the spatial footprint of liquid overflow that is typically obscured by snow and invisible to the naked eye. The UAS-based GPR had an RMSE of 5 cm for ice thickness varying from 20-60 cm. However, this depends on the ice dielectric constant of 2, which is not consistent with the type of ice measured.

When comparing the UAS-GPR system with ground-based GPR and ice cores nearby, we found a measurable bias that requires more investigation. More work is needed to uncover sources of potential error in UAS-based GPR.

CHAPTER 1. INTRODUCTION

Rural Alaska depends on winter ice roads to connect villages. In Southwest Alaska, Bethel is the central hub for many satellite villages. A town hub like Bethel provides critical services such as a regional airport, hospital, food and supplies, and more. Other places in Alaska, such as Tanana Village, are connected during winter via an ice road to the Alaska highway system. These ice roads are a seasonal umbilical cord that rural Alaska depends on. These ice roads support personal and commercial traffic. To that end, commercial traffic can be as heavy as large tractor-trailers bringing essential food or building supplies and large, heavy equipment for summer development. The ice roads can be tens of miles long or nearly 100 miles long (outside of Bethel); thus, maintaining these roads open to traffic despite inclement weather and changes to the ice is daunting.

The safety of driving on ice roads varies in time and space. Snow drifts on ice roads are common obstacles that are reasonably easy to spot and avoid. On the contrary, thin ice and subsnow slush (overflow) are impossible or very difficult to spot from a safe distance. During the fringes of ice road season, local ice hazards can develop unexpectedly and abruptly. Climate change is another wild card that plays on ice roads. Unseasonal warm temperatures in winter with above-freezing temperatures events, or even rain, can swiftly and heterogeneously degrade ice road safety.

Typically, ice road safety is inspected using an auger to drill a hole into the ice and measure the ice thickness (h), including examining the ice quality and measuring the effective ice thickness. Gold's formula uses effective ice thickness to calculate the ice road load bearing. Poorly bonded ice should not be counted as part of the ice thickness that feeds the Gold's formula. Thus, mapping the variability of ice thickness or subsnow overflow requires putting a person on the ice at risk over the area in question. Furthermore, traversing an ice road, auguring, and collecting ice thickness is labor-intensive and time-consuming. Ice coring is a point measurement. It only describes the ice parameters, such as thickness and quality, at the measurement point and provides little to no insight into the ice conditions further away from the coring location. This is important when the ice quality and thickness are spatially heterogeneous, and a single ice core would not capture that variability.

Ground-penetrating radar (GPR) is a promising instrument that can provide insight into the ice without manual ice auguring. E M. Richards (2021) tested a GPR over ice roads on the Yukon River and the Tanana River near Fairbanks, Alaska. The GPR provides continuous measurements as opposed to augured point measurements. E M. Richards showed that GPR surveys provided accurate mean absolute error (MAE) measurements of 3.6-5.8 cm for ice thickness of 0.91-1.57 m compared with manually augured ice coring, assuming a constant radar velocity. The GPR provided a map of ice thickness variability over the surveyed areas. However, the root mean square errors (RMSE) of the GPR compared with the manual measurements showed that variability in snow conditions affects the GPR data's accuracy. This was attributed to uneven snow cover and the effect on the path of the radar pulse. The GPR system used by E M. Richards was towed on a wheeled cart. This made it difficult to pull the cart over rough ice surfaces and keep a leveled radar with a consistent distance from the surface. The GPR does not provide accurate ice measurements when liquid water is between the radar and the ice.

In addition to the risk of thin ice to ice road stakeholders, subsnow slush, often under unperturbed snow, is impossible to identify to the naked eye and can trap heavy equipment, vehicles, or

snowmachines, and is very dangerous, particularly at very cold temperatures. Gusmeroli et al. (2012) pointed out the effectiveness of a GPR system in identifying subsnow slush. Gusemeroli pointed out that the radar reflection signal strength from the liquid-ice interface is twice as strong as from the snow-ice interface.

Thus, GPR can provide accurate ice thickness information where there is no overflow and map areas where overflow is present. However, both GPR applications described above are systems towed on either a wheeled cart or sled and require being present over the ice. A GPR system mounted on an unmanned aircraft system (UAS) would enable conducting ice assessments without placing a person at risk. Therefore, this project explores the utility and experience of using an airborne GPR mounted on a UAS to assess ice thickness and map subsnow slush.

Ground-based GPR has decades of heritage in the ice road community and has become increasingly popular due to the non-invasive nature of the measurement technique and its ability to rapidly survey ice thickness over large areas (Annan A.P., 2016). GPR instruments small enough to mount on UAS came to market in the late 2010s (Li C.J. et al., 2016; Colorado, J. et al., 2017; Burr, R. et al., 2018) and present an exciting opportunity for ice road surveys, acquiring GPR data without sending a person and/or vehicle out on the ice.

Moving the GPR sensor from the ground to an airborne platform introduces new sources of error to the measurement process. Because no instrument operator is necessarily present where the GPR data is being acquired, there is potentially little to no information about snow thickness and quality on top of the ice. Increased uncertainty about snow conditions will cause increased uncertainty in the ice measurement, mainly if the snow is thin enough such that the air-snow and snow-ice interfaces are closer than the resolution of the radar, so they cannot be independently resolved. Additionally, the altered survey geometry will change the apparent shape of sloping radar reflectors in un-migrated radar data. Migration of UAS-based radar data is more difficult than on ground-based radar data because the standard migration routines that assume homogenous velocity cannot be used, particularly in cases where there is significant variation in ice thickness and/or UAS flight height.

Transitioning to a UAS-based measurement also increases the likelihood of failing to detect a bottom-of-ice interface. New sources of loss are introduced along the radar path; geometric spreading in the air and reflection at the air-ground interface reduce the amount of power transmitted into the subsurface. This can be an issue in overflow conditions when liquid water on top of the ice provides a significant dielectric contrast reflecting most of the incident power.

Here, we seek to measure and quantify some of these new sources of error by comparing UAS-based GPR data with ground-based GPR and manual ice thickness measurements. Additionally, we compare the quality (in a semi-quantitative sense) and UAS-based GPR data to ground-based GPR data and identify scenarios in which one of the two methods is more appropriate.

CHAPTER 2. GPR SYSTEM AND DATA GATHERINGS

2.1. The GPR and aircraft system

For this project, we used the Aero Zone 500, manufactured by Radar Systems. The radar frequency is 200-900 MHz, centered at 500 MHz. The radar has a 12 dB fractional bandwidth of 140%. The GPR was mounted on a DJI Matrice 300 RTK manufactured by DJI. The radar dimensions are (L x W x H): 41 x 31 x 16 cm and weigh 2.1 Kg.

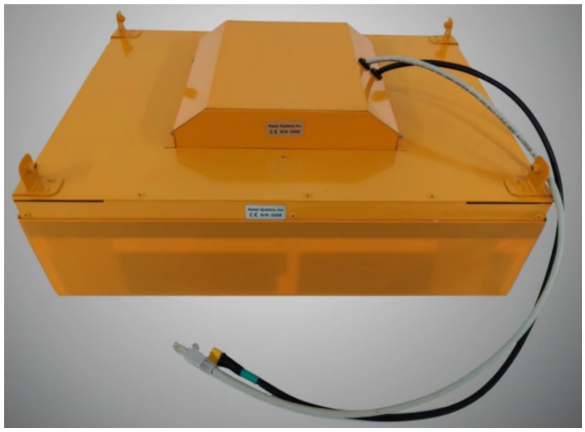

Figure 1. The Zone 500 GHz radar

Data are collected and stored by a dedicated device, a single board, the Skyhub (SPH Inc.). The Skyhub also has an altimeter, which together commands the aircraft to maintain a fixed altitude from the ground.

The Alaska Department of Transportation & Public Facilities (DOT &PF) flew the GPR on a DJI Matrice 300. This aircraft has marketed endurance of sub-hour endurance and can carry as much as 2.7 Kg. However, with the GPR system, the endurance was closer to 10 minutes.

Figure 2. The Zone 500 radar is mounted to the DJI Matrice 300. The Radar and aircraft are seen after landing and between flights.

2.2. Flying the GPR on the Matrice 300 UAS

We tested flying the GPR in the following flight configurations:

Table 1. A summary of experimenting with aircraft flight parameters

Aircraft ground speed (m/s)	Altitude above the ground (m)
1	1
1	1
2	3
2	5

We chose a flight envelope of 2 meters above the surface and 2 m/s ground speed to balance aircraft flight safety above the ground, GPR signal strength, and flight efficiency. The aircraft's battery enabled surveys of about 8 minutes, which is about 1 km. Surveying the Tanana Lakes, seen in Figure 3, encompassed three survey strips, with four passes each. Two flights were able to cover the three survey patches.

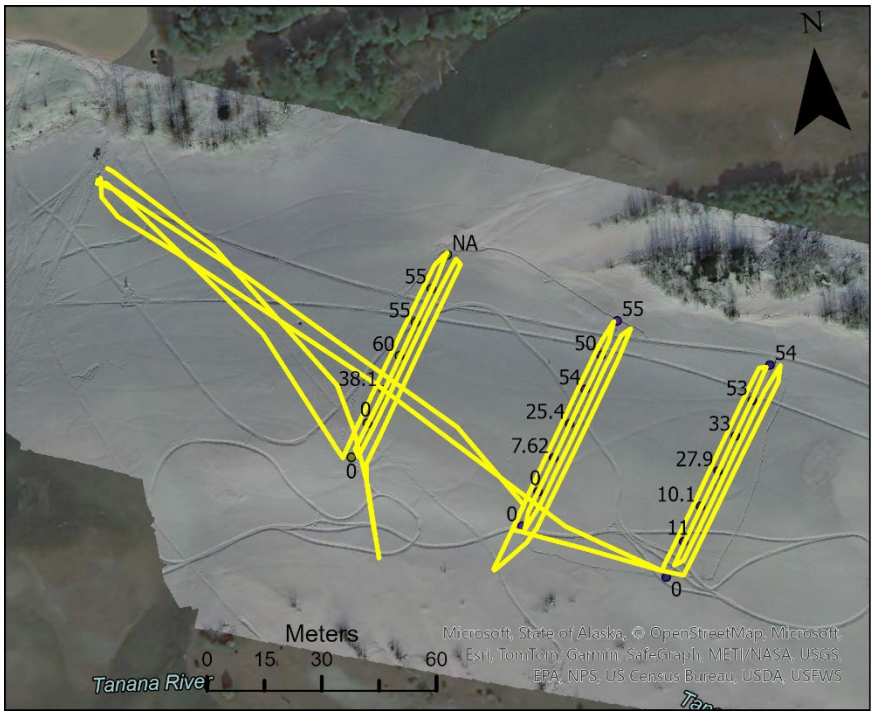

Figure 3. A map of a UAS flight passes over Tanana Lakes with the background of an orthomosaic from the UAS imagery and a satellite background.

2.3. UAS GPR data collection

Our team acquired over 14 line-km of UAS-based GPR data in Spring 2023 (Figures 6 and 7) with a Zond Aero 500 GPR instrument. Initial data acquisition targeted lake ice, which we expected to be a homogeneous and relatively easy (compared to river ice) target for the radar, based on previous studies

(Annan, A.P. et al., 2016 and Richards, E.M., 2021). Figure 4 depicts a radargram over the Tanana Lakes. This survey was of lake ice with no snow cover.

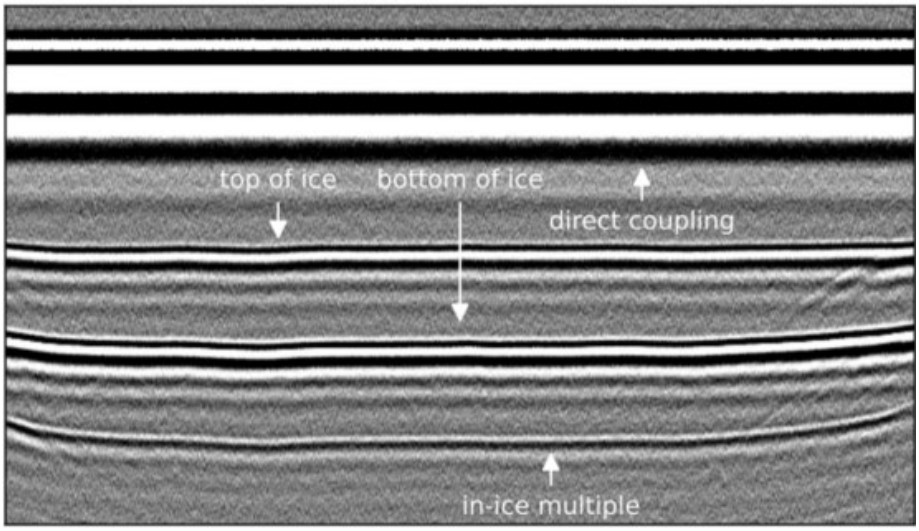

Figure 4, an example of a radargram from Tanana Lakes with distinct top of ice and bottom of ice reflection (site D in Figures 7 and 8)

We began targeting river ice after acquiring data at Chena Lake and Tanana Lakes and building operational proficiency. Three river ice surveys were completed on the Chena River (Figure 8, C and B) and Tanana River (Figure 8, F). Figure 5 depicts a radargram over the Chena River (Figure 8C), with snow cover, some snowmachine tracks, and no observed overflow. This radargram of the river nicely delineates the different layers, and one can see that the ice is thicker where the distance between the top and bottom of the ice is the widest.

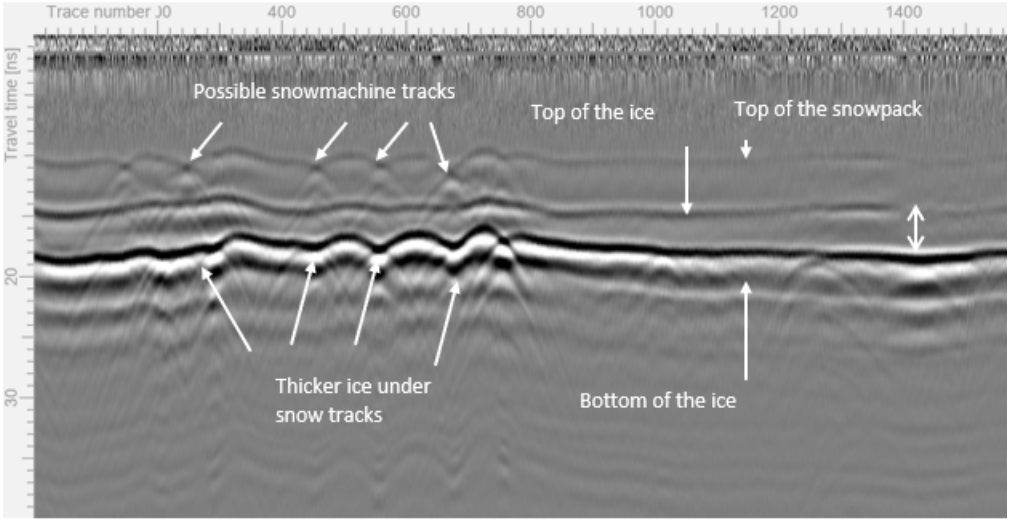

Figure 5. An example of a radargram of the Chena River ice with a snowpack and no overflow.

Analyzing GPR data from the Tanana River cross-section, where overflow below the snow and above the ice is present, was a more challenging target for the GPR. As shown in Figure 6, below, the figure is much noisier and harder to delineate the top and bottom of the ice. This was much easier in the Tanana Lakes with no snow, and the Chena River with snow, where the ice was distinct and easy to pinpoint (Figures 4 and 5). On the contrary, in the case of river ice with snow and overflow, the top of the ice is reasonably identifiable, but the bottom is indistinguishable.

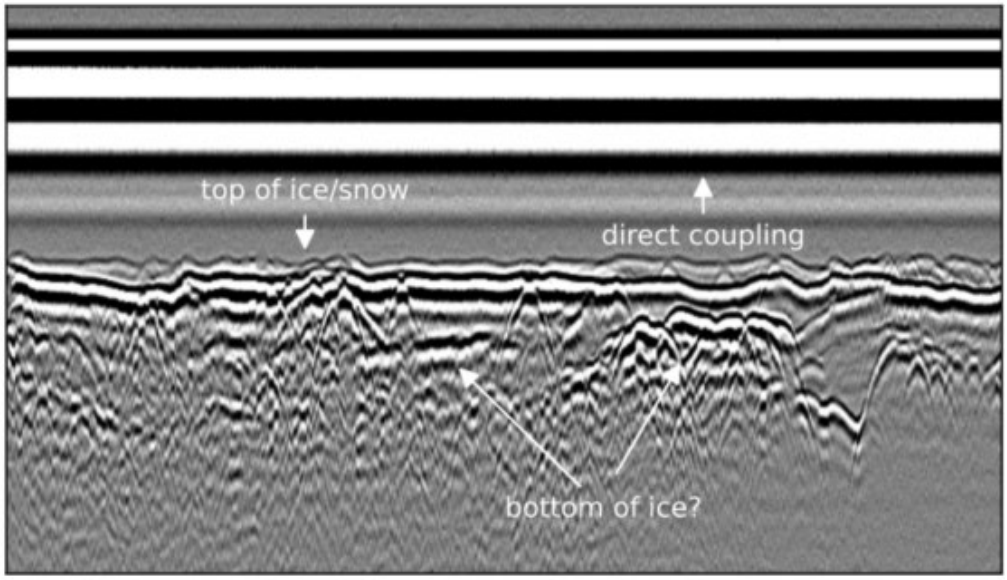

Figure 6 depicts an example of a radargram from Tanana River lacking a distinct bottom of the ice reflection (site F in figures 7 and 8).

2.4. Manual ice thickness measurements

We used ice augers and tape to measure the thickness of the ice and snow, which provided ground truthing for the GPR data.

CHAPTER 3. RESULTS AND ANALYSIS

3.1. Study sites

The UAS-based GPR was flown over six different sites (Figure 7) to gain experience operating the radar and determining the ideal conditions for measuring ice thickness from a drone.

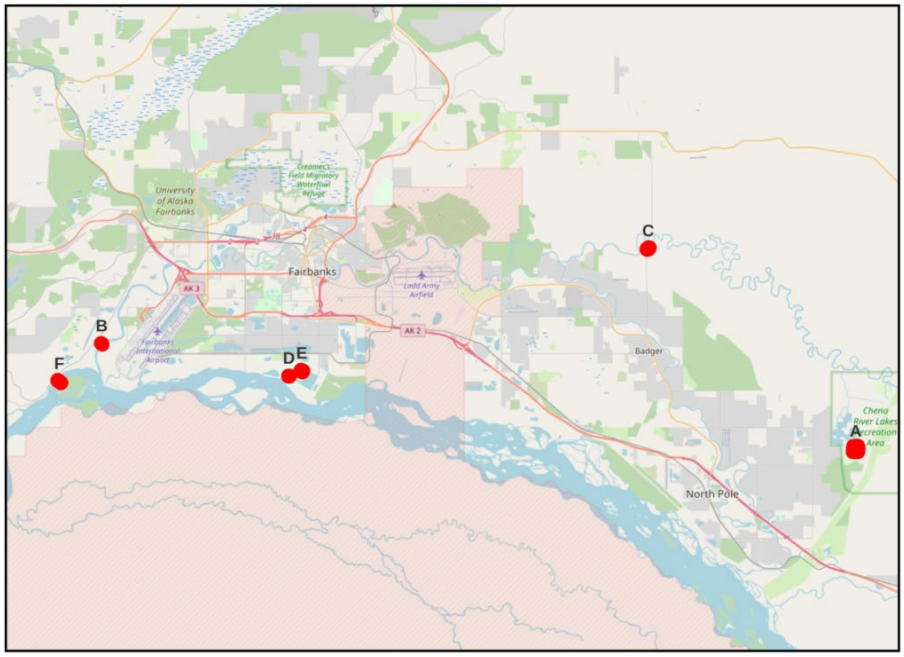

Figure 7. GPR survey sites in and around Fairbanks, Alaska.

With the aircraft survey speed of 2 m/s and about 8 minutes of flying time, the survey geometry had to account for the desired area to map while accounting for the flight duration. Another critical factor is the distance the aircraft needs to traverse from the takeoff site to the survey site and back (not seen in Figure 8). In Figure 8, panel A, the aircraft surveyed a relatively large box of almost 200 x 200 meters. However, in other locations where the aircraft had to traverse to the survey site, we picked three or four cross-section areas of the water body, as seen in panels C and E in Figure 8.

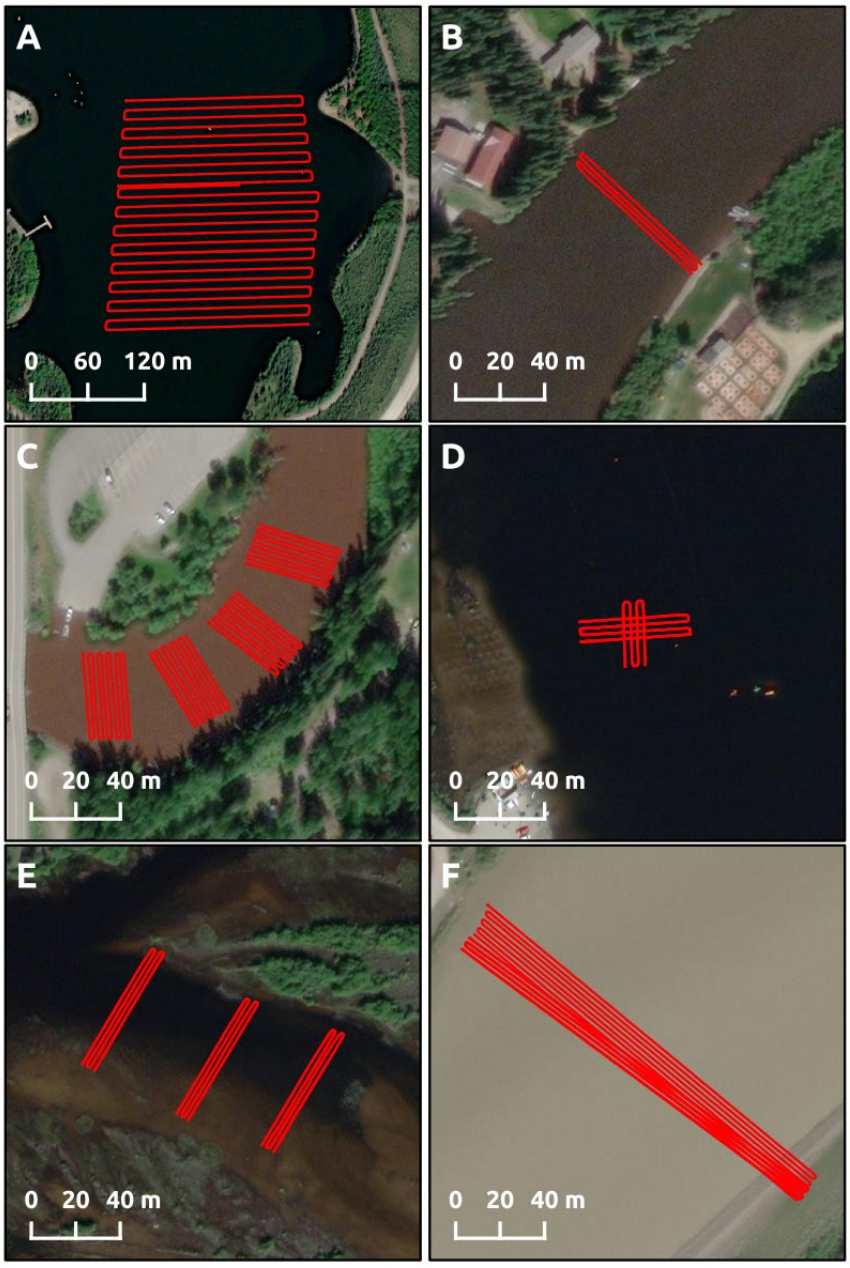

Figure 8 depicts six UAS-GPR survey areas (A through F) as charted in Figure 7. In these six survey sites, different UAS-based GPR survey geometries were tested.

3.2. Comparison of UAS-based and ground-based GPR

At the Chena River near the Nordale field site (location C in Figures 7 and 8), we compared the interpreted in-ice travel time from 400 MHz ground-based GPR surveys to the nearest UAS data (Figure 9), usually within 1 meter. The ground-based GPR shows a bias to longer travel times with a median difference between the two methods of 0.6 ns, corresponding to 5 cm of ice thickness at an assumed

dielectric constant of 3.15. The apparent travel-time difference between the two datasets is due to an interpretive bias. Without more experimentation, it is difficult to make any concrete statements about the source of the difference. It should be noted that the ground-based and UAS-based radars have different center frequencies (400 and 500 MHz, respectively), which could lead to differences in the resultant data. Future testing should include the operation of the same GPR instrument on the ground and from a UAS along the same path to enable a more direct comparison of the data products.

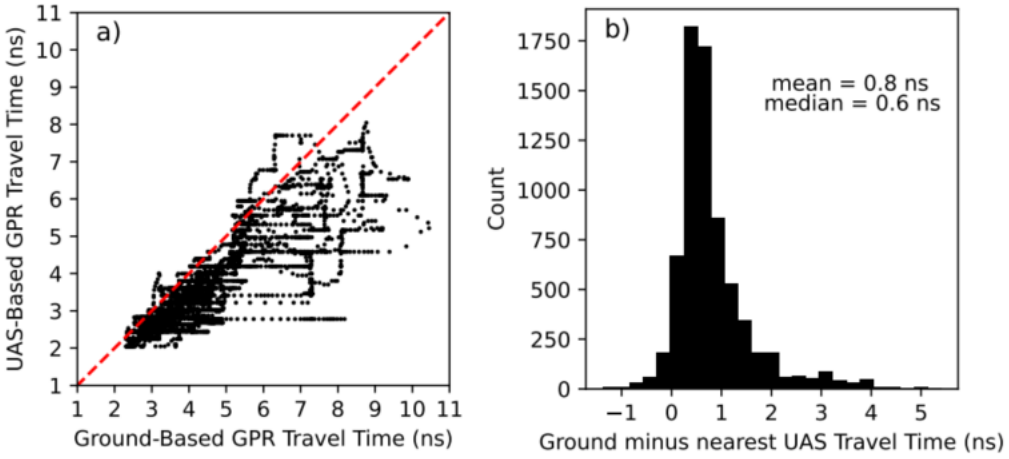

Figure 9. A comparison between UAS and ground-based radar wave travel time.

3.3. Calibration of UAS-based GPR with manual ice thickness measurements

At the Chena River near the Nordale site (site C in Figures 7 and 8), we compared manual ice thickness measurements from augured holes to ground and UAS-based radar measurements. A least-squares fit of the manual ice thickness measurements to the nearest in-ice GPR travel times yields a best-fit dielectric constant of 2.0 for the UAS-based data and 3.3 for the ground-based data (Figure 10).
This significant discrepancy between the best-fit dielectric constant in the UAS and ground-based data should be a target of future investigation. A dielectric constant 2.0 would imply significant (tens of percent) gas content in the ice, which was not found in the ice core measurements. The dielectric constant of 3.3 derived from fitting the ice core thicknesses and the ground-based GPR measurements is much more reasonable for a relatively pure ice mass. These initial results suggest that the ice thickness measurements derived from the UAS-based GPR data systematically underestimate the thickness of the ice. It remains to be seen whether this is an instrumental effect or an issue in the interpretation of the radar data.

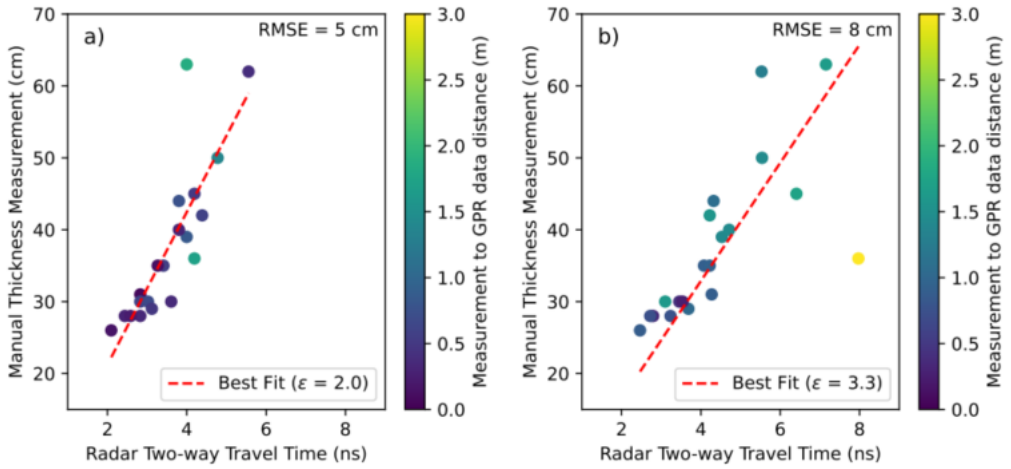

Figure 10. Comparing UAS-based GPR on the left and ground-based GPR on the right with manual ice coring (y-axis).

3.4. Ice Surface Reflection Amplitude

While acquiring UAS-based GPR data, we noticed a correlation between the amplitude of the apparent ice surface reflection and the presence of overflow on the ice. This relationship is not unexpected; a layer of liquid water will provide a large dielectric contrast with the air, snow, or ice above it, leading to a strong reflection.

We investigated the potential of surface reflection amplitude to be used as a proxy for detecting areas with overflow by interpolating the maximum amplitude of the surface reflection with an inverse distance weighting scheme and comparing the amplitude grids to in-situ observations of overflow (Figure 11). The amplitude grids show strong spatial variations that are correlated with observed overflow. Red dots in panel E, are where subsnow overflow conditions were observed. Pannel B and F do not have manual measurements, so the presence of overflow could not be confirmed. This method shows promise for mapping areas of subsnow overflow before sending equipment onto the ice.

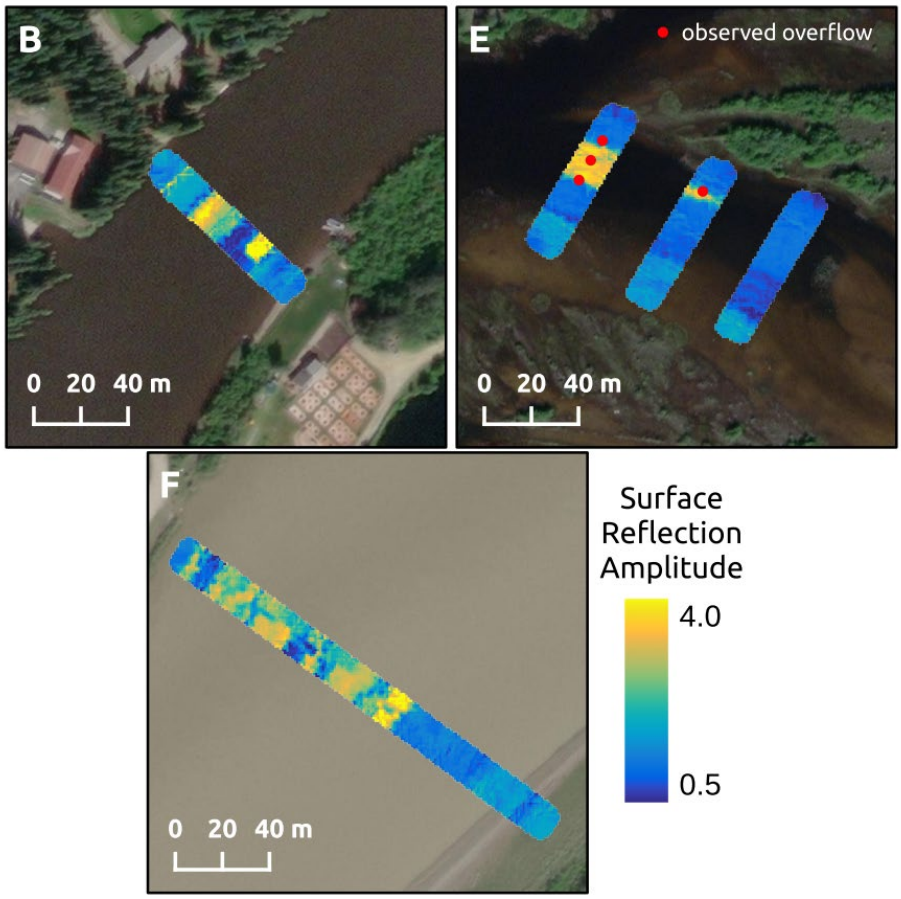

Figure 11 depicts three UAS-GPR survey areas (B, E, and F) as described in Figure 7. The color bar depicts ice surface reflection amplitude. The high amplitude (about 4 and in yellow) is probably due to the air-to-water change in dielectric properties, which seems to indicate of subsnow liquid overflow. These are overflow conditions identified under the snow. Where the amplitude is low (0.5- blue), it is identified with no overflow conditions. Red dots are where overflow was confirmed with a manual measurement.

CHAPTER 4. DISCUSSION

This study shows that drone-based GPR can survey river ice and provide information comparable in quality to ground GPR without "putting boots on the ground." In contrast to manual GPR and the challenge of keeping it leveled over rough ice, drone GPR handles rough surfaces better by keeping the UAS and GPR leveled. However, we did not encounter extreme rough ice to challenge the system. The drone-based GPR had an RMS of 8 cm for 60 cm of ice. However, this assumed a dielectric property of 2, suggesting a type of ice high in gas content.

This preliminary study opens several avenues for future work. Moving forward, the most crucial task will be understanding the source of the travel-time discrepancy between the UAS-based and ground-based GPR data. The dielectric constant regression performed using manual ice thickness measurements suggests that this discrepancy is caused by an underestimate in the travel time derived from the UAS-based radar data. It remains to be seen whether this is an instrument/observational effect or whether this is due to an error in the interpretive process.

CHAPTER 5. REFERENCES

Annan, A.P., Diamanti, N., Redman, J.D. and Jackson, S.R., 2016. Ground-penetrating radar for assessing winter roads. *Geophysics*, *81*(1), pp.WA101-WA109.

Burr, R., Schartel, M., Schmidt, P., Mayer, W., Walter, T. and Waldschmidt, C., 2018, April. Design and Implementation of a FMCW GPR for UAV-based Mine Detection. In *2018 IEEE MTT-S International Conference on Microwaves for Intelligent Mobility (ICMIM)* (pp. 1-4). IEEE

Colorado, J., Perez, M., Mondragon, I., Mendez, D., Parra, C., Devia, C., Martinez-Moritz, J. and Neira, L., 2017. An integrated aerial system for landmine detection: SDR-based Ground Penetrating Radar onboard an autonomous drone. *Advanced Robotics*, *31*(15), pp.791-808

Gusmeroli, A. and Grosse, G., 2012. Ground penetrating radar detection of subsnow slush on ice-covered lakes in interior Alaska. *The Cryosphere*, *6*(6), pp.1435-1443.

Li, C.J. and Ling, H., 2016, June. High-resolution, downward-looking radar imaging using a small consumer drone. In *2016 IEEE International Symposium on Antennas and Propagation (APSURSI)* (pp. 2037-2038). IEEE.

Richards, E.M., 2021. *An evaluation of GPR techniques for analyzing the safety of Interior Alaskan ice roads under varying river ice and environmental conditions*. University of Alaska Fairbanks.